Applied Microbiology and Biotechnology
https://doi.org/10.1007/s00253-023-12581-6

BIOTECHNOLOGICALLY RELEVANT ENZYMES AND PROTEINS

Improvement of *Cellulomonas fimi* endoglucanase CenA by multienzymatic display on a decameric structural scaffold

Matías R. Iglesias Rando[1,2] · Natalia Gorojovsky[1,2] · Vanesa Zylberman[3] · Fernando A. Goldbaum[3,4,5] · Patricio O. Craig[1,2]

Received: 9 February 2023 / Revised: 27 April 2023 / Accepted: 6 May 2023

Abstract

The development of multifunctional particles using polymeric scaffolds is an emerging technology for many nanobiotechnological applications. Here we present a system for the production of multifunctional complexes, based on the high affinity non-covalent interaction of cohesin and dockerin modules complementary fused to decameric *Brucella abortus* lumazine synthase (BLS) subunits, and selected target proteins, respectively. The cohesin-BLS scaffold was solubly expressed in high yield in *Escherichia coli*, and revealed a high thermostability. The production of multienzymatic particles using this system was evaluated using the catalytic domain of *Cellulomonas fimi* endoglucanase CenA recombinantly fused to a dockerin module. Coupling of the enzyme to the scaffold was highly efficient and occurred with the expected stoichiometry. The decavalent enzymatic complexes obtained showed higher cellulolytic activity and association to the substrate compared to equivalent amounts of the free enzyme. This phenomenon was dependent on the multiplicity and proximity of the enzymes coupled to the scaffold, and was attributed to an avidity effect in the polyvalent enzyme interaction with the substrate. Our results highlight the usefulness of the scaffold presented in this work for the development of multifunctional particles, and the improvement of lignocellulose degradation among other applications.

Key points

- *New system for multifunctional particle production using the BLS scaffold*
- *Higher cellulolytic activity of polyvalent endoglucanase compared to the free enzyme*
- *Amount of enzyme associated to cellulose is higher for the polyvalent endoglucanase*

Keywords BLS · Scaffold · Artificial cellulosome · Multienzymatic complex · Cellulase

✉ Patricio O. Craig
pocraig@hotmail.com; pocraig@qb.fcen.uba.ar

[1] Departamento de Química Biológica, Facultad de Ciencias Exactas y Naturales, Universidad de Buenos Aires, Intendente Güiraldes 2160 (CP 1428), Buenos Aires, Argentina

[2] CONICET-Universidad de Buenos Aires, Instituto de Química Biológica de la Facultad de Ciencias Exactas y Naturales (IQUIBICEN), Intendente Güiraldes 2160 (CP 1428), Buenos Aires, Argentina

[3] Inmunova SA, Gral. San Martín, 25 de Mayo 1021 (CP 1650), Villa Lynch, Buenos Aires, Argentina

[4] Fundación Instituto Leloir, IIBBA-CONICET, Av. Patricias Argentinas 435 (CP 1405), Buenos Aires, Argentina

[5] Centro de Rediseño e Ingeniería de Proteínas (CRIP), UNSAM Campus Miguelete, 25 de Mayo y Francia (CP 1650), Gral. San Martín, Buenos Aires, Argentina

Introduction

Lignocellulose is the most abundant renewable natural resource on the planet and is an excellent substrate for biofuel production. The current industrial production of second generation bioethanol involves the hydrolysis of lignocellulose using non-complexed (free) cellulolytic enzymes (Wilson 2009). Despite the ongoing efforts, this process remains non-competitive with fossil fuel due to the high recalcitrance of the lignocellulosic substrate, and the low efficiency and high cost of the enzymes used (Himmel et al. 2007). The development of new strategies to enhance the enzymatic degradation of lignocellulose is crucial for the economic viability of biofuel production.

The multiple display of proteins in polymeric scaffolds is an emerging technology with numerous biotechnological applications. It could be used to increase the interaction

Published online: 22 May 2023

strength of domains with their target ligands through an avidity effect (Plückthun and Pack 1997; Gestwicki et al. 2002; Zhang et al. 2004; Banerjee et al. 2010), to increase the immunogenicity of antigens for vaccine development (Ludwig and Wagner 2007; Jennings and Bachmann 2008; Mejía-Méndez et al. 2022), and to colocalize metabolic cascade enzymes to increase their activity through synergistic effects (Jørgensen et al. 2005; Dueber et al. 2009; Agapakis et al. 2012; Garbett and Bretscher 2014), among other applications.

A paradigmatic example of a scaffold-based multienzymatic complex found in nature is the cellulosome produced by some anaerobic microorganisms. Cellulosomes are the most efficient machinery for degrading lignocellulose. These multienzymatic complexes group different lignocellulolytic enzymes on a scaffold protein through high-affinity non-covalent interactions between cohesin and dockerin domains present in the structure of the scaffold and enzymes, respectively (Artzi et al. 2017). The enzyme diversity of the cellulosome includes different types of endoglucanases, exoglucanases, xylanases, and other enzymes. The cellulosome produced by *Clostridium thermocellum* has been one of the most studied. It has been established that the cellulose degradation activity of this multienzymatic complex is approximately 12-fold higher than that of an equivalent amount of its enzymes free in solution (Krauss et al. 2012). Enzyme proximity and substrate targeting effects, produced by the colocalization of different enzymes and cellulose binding domains in the structure of the cellulosome, have been proposed to explain the cellulolytic synergism of the different cellulosomal modules (Bayer et al. 1983; Shoham et al. 1999). The cellulosomes represent a useful machinery for lignocellulose degradation. However, their production on an industrial scale is problematic by difficulties in the production and extraction of large amounts of these complexes from their natural source and limitations in their recombinant expression. In particular, the recombinant expression yield of the natural scaffold protein is very low due to its large size and repetitive nature (Gunnoo et al. 2016). Extensive work has been done to understand the basis of the increased activity of cellulosomes through the production of designer cellulosomes (Mingardon et al. 2007a,b; Moraïs et al. 2012; You and Zhang 2014; Arfi et al. 2014; Stern et al. 2016; Davidi et al. 2016; Bayer 2017). In these studies, truncated or chimeric scaffold variants heterologously expressed in bacteria and yeast have been used. However, the production of large amounts of cellulosomes with similar size and activity as the natural ones has been limited. Alternative approaches for the production of artificial cellulosomes involve the use of nanoparticles (Blanchette et al. 2012; Lu et al. 2019), DNA (Sun et al. 2014; Sun and Chen 2016), and self-assembling oligomeric proteins (Mitsuzawa et al. 2009; Moraïs et al. 2010) as scaffolds.

Brucella abortus spp. lumazine synthase (BLS) is an enzyme that catalyzes an intermediate step in the biosynthesis of riboflavin, and exhibits remarkable structural features that stimulated its use as scaffold for the display of a variety of peptides and proteins (Zylberman et al. 2004; Bonomi et al. 2010). It has a decameric structure formed by a 17 kDa subunit arranged as a dimer of pentamers (Zylberman et al. 2004; Klinke et al. 2005, 2007). It is highly stable and resistant to the action of proteases and chaotropic agents like urea. Although it is possible to couple proteins to the structure of BLS by recombinant fusion (Craig et al. 2005; Bellido et al. 2009; Alvarez et al. 2013; Mejias et al. 2013; Rossi et al. 2015; Hiriart et al. 2017; Berguer et al. 2022), these constructs are frequently expressed as inclusion bodies in *Escherichia coli* and require refolding steps that do not always succeed. Non-covalent coupling methods using heterodimeric partners recombinantly fused to the scaffold subunits and target proteins are useful to overcome the problems associated with the concomitant folding and association of protein modules on oligomeric particles (Jennings and Bachmann 2008; Craig et al. 2012). A method using heterodimeric coiled-coil peptides was successfully developed previously for the non-covalent coupling of proteins to BLS structure (Craig et al. 2012). However, the scaffold is expressed in inclusion bodies and a solubilization step in urea is required prior to the coupling step.

In this work, we develop a novel system for the production of multifunctional particles based on the non-covalent coupling of proteins to BLS through high-affinity cohesin and dockerin modules recombinantly fused to BLS and the target proteins, respectively. To evaluate the usefulness of the cohesin-BLS fusion (cBLS) as a scaffold for the polymeric display of enzymes, we used the catalytic module of the *Cellulomonas fimi* endoglucanase CenA. The polymeric display of this enzyme on the cBLS structure produced structurally and functionally stable multienzymatic complexes with higher cellulolytic activity and higher cellulose association properties for the insoluble phosphoric acid swollen cellulose (PASC) and Avicel substrates, compared to the non-complexed enzyme. These results make cBLS an attractive scaffold for multifunctional particle development, such as the production of artificial cellulosomes, and other biotechnological applications.

Materials and methods

Molecular cloning

The coding sequence of *C. thermocellum* cohesin-2 domain of CipA (Uniprot ID: Q06851, region 181–328) was obtained by gene synthesis (Genscript, Piscataway, NJ, USA), and recombinantly fused to the sequence of the

N-terminal end of BLS in the pET11a vector (Novagen, Madison, WI, USA). For this aim, we replaced the coding sequence of the first nine residues of BLS, by the coding sequence of cohesin to obtain the pet11a_cBLS construct (GenBank Accession #OQ551415). The cassette mutagenesis strategy used to build this construct was similar to the one used previously for the construction of other BLS fusions (Laplagne et al. 2004), with *Nsi*I/*Afl*II sites added to the 5′ and 3′ ends of the fused target. The final construct included a flexible and hydrophilic pentapeptide linker of sequence GSGSG joining the cohesin and BLS modules.

The coding sequence of the catalytic domain of *C. fimi* CenA endoglucanase ($CenA^{CD}$, Uniprot ID: P07984, region 160–449) was obtained by PCR amplification of a synthetic biology construct from the Registry of Standard Biological Parts (http://parts.igem.org/Main_Page, part#: BBa_K118023), whereas the coding sequence of the dockerin domain of endo-1,4-β-xylanase Xyn10B from *C. thermocellum* (Uniprot ID: P51584, region 730–791) was obtained by gene synthesis (Genscript, Piscataway, NJ, USA). The recombinant fusion of this dockerin to the C-terminal end of $CenA^{CD}$ was done for the production of the $CenA^{CD}$d fusion protein. We used *Nde*I/*Afl*II restriction sites added to the 5′ and 3′ ends of $CenA^{CD}$, and *Afl*II/*Nhe*I sites added to the 5′ and 3′ ends of dockerin, and ligated both genes in the pET11a vector. Primers were designed to include a histidine tag at the N-terminal end of $CenA^{CD}$, and a peptide linker of sequence GSGSG joining $CenA^{CD}$ and dockerin modules in the final pet11a_$CenA^{CD}$d construct (GenBank Accession #OQ551414).

The codon usage of the cohesin and dockerin genes was optimized for expression in *E. coli*. PCR amplifications were performed using Pfu DNA polymerase (PB-L Productos Biológicos, Bernal, Buenos Aires, Argentina). PCR products and vectors, digested with *Nsi*I, *Afl*II, and *Nhe*I restriction enzymes (NEB, Ipswich, Massachusetts, USA), were purified using Promega Wizard™ SV Gel and PCR Cleanup System (Promega, Madison, WI, USA). Ligation was performed with T4 DNA ligase (NEB, Ipswich, Massachusetts, USA). Competent *E. coli* DH5α cells (Thermo Fisher Scientific, Waltham, MA, USA) were used for plasmid transformation and amplification.

Protein expression and purification

The pet11a_cBLS and pet11a_$CenA^{CD}$d vectors were transformed in BL21 (DE3) competent cells (Thermo Fisher Scientific, Waltham, MA, USA) for protein expression. Cultures of these clones in 0.5–1 L Luria–Bertani broth supplemented with the appropriate antibiotic (100 mg/L of ampicillin) were grown at 37 °C for approximately ~ 3 h, and after reaching an OD at 600 nm of ± 0.7–1.0, the bacterial cells were induced with isopropyl-1-thio-β-D-galactoside (IPTG). Induction of $CenA^{CD}$d was carried out using 0.1 mM IPTG for 4 h at 20 °C, whereas cBLS induction was done with 1 mM IPTG, overnight at 30 °C. Cells were harvested by centrifugation at 4500 × g for 15 min. The pellets were resuspended in 15 mL of 50 mM Tris–HCl, pH 7.5 buffer, containing 1 mM phenylmethylsulfonyl fluoride (PMSF), and 5 mM imidazole. Cells were sonicated, centrifuged at 25,000 × g for 15 min, and the supernatant was filtered with a polyethersulfone (PES) syringe filter of 0.45 µm pore size (Sartorius, Goettingen, Germany). His-tagged $CenA^{CD}$d was purified by affinity chromatography on a 1 mL HisTrap™ high performance column, followed by a size-exclusion chromatography step using a Superdex 200 column. cBLS was purified using a Q-Sepharose anion exchange column, followed by size-exclusion chromatography on a Superdex 200 column, and monoQ anion exchange chromatography steps. All columns and media used for protein purification were from GE Healthcare Bio-Sciences AB (Uppsala, Sweden). Chromatographic purifications were done on a DIONEX Ultimate 3000 HPLC system (Thermo Fisher Scientific, Waltham, MA, USA). The concentration of the purified proteins was measured by UV absorbance at 280 nm, using the extinction coefficient calculated by the Protparam tool (https://web.expasy.org/protparam/). The proteins were subsequently frozen with liquid nitrogen and stored at − 80 °C.

$CenA^{CD}$d coupling to cBLS

Coupling of $CenA^{CD}$d to cBLS was carried out by incubating both proteins in Tris-buffered saline (50 mM Tris, 150 mM NaCl, pH 7.5) supplemented with 0.05% Tween 20 and 2 mM $CaCl_2$ (TBS-TC buffer) at 4 °C for 1 h. The production of cBLS-$CenA^{CD}$d complexes of different multiplicity (*n*) was carried out using different stoichiometric amounts of $CenA^{CD}$d and cBLS. Equimolar amounts of $CenA^{CD}$d and cBLS subunits were used for the saturation of cBLS decameric scaffold, producing complexes with 10 $CenA^{CD}$d molecules per decameric nanoparticle (cBLS-$CenA^{CD}d_{(10)}$). On the other hand, an excess of 10 cBLS subunits per 1 $CenA^{CD}$d molecule was used for the production of complexes with an average of 1 $CenA^{CD}$d per decameric nanoparticle (cBLS-$CenA^{CD}d_{(1)}$).

Size exclusion chromatography coupled to static light scattering (SEC-SLS)

The molecular mass (Mr) of the proteins and complexes used in this work were determined on a PD2100 light scattering instrument (Precision Detectors, Bellingham, MA, USA) tandemly connected to a high-performance liquid chromatography system, including a Waters 486 UV detector (Waters Corporation, Milford, MA, USA), and a LKB 2142 differential refractometer (LKB, Bromma, Sweden). The

protein samples were run on a Superose 6 increase 10/300 GL column (GE Healthcare Bio-Sciences AB, Uppsala, Sweden). cBLS, CenA^{CD}d, and cBLS-CenA^{CD}d complexes were eluted in TBS-TC buffer. All separations were performed at a 0.5 mL/min flow rate. The elution was monitored by measuring the static light scattering at 90° (SLS), the UV absorption at 280 nm (UV_{280}), and the refractive index (RI) signals. The data was recorded on a personal computer and analyzed with the Discovery32 software supplied by Precision Detectors (Bellingham, MA, USA). The Mr of each sample was calculated by the analysis of the SLS, RI, and UV signals, and comparison of the results with the ones obtained for BSA as a standard (Mr 66.5 kDa). The UV extinction coefficients at 280 nm of CenA^{CD}d and the cBLS subunits (73,130 and 17,420 M^{-1} cm^{-1}, respectively), were calculated using the Protparam tool (https://web.expasy.org/protparam/). The extinction coefficient of the decavalent cBLS-CenA$^{CD}d_{(10)}$ protomers (90,550 M^{-1} cm^{-1}) was calculated as the sum of the extinction coefficients of CenA^{CD}d and the cBLS subunits.

CD (circular dichroism) spectrum and thermal denaturation assay

The CD spectra in the far UV region (250–200 nm) of cBLS, CenA^{CD}d, and cBLS-CenA^{CD}d complexes in TBS-TC buffer were measured on a J-810 spectropolarimeter (Jasco, Tokyo, Japan) using quartz cuvettes of either 1 or 5 mm path length. The results were expressed in units of molar ellipticity (° cm^2 $dmol_{prot}{}^{-1}$) per dmol of protein subunits.

The heat-induced denaturation of the protein samples was monitored by measuring the CD signal at 222 nm as a function of temperature. The samples were slowly heated from 20 to 95 °C at 4 °C/min using a Peltier device (Jasco, Tokyo, Japan). The molar ellipticity at 222 nm was measured every 0.5 °C. The melting temperature (T_m) of each protein was calculated from the middle point of the unfolding curve measured. Due to the irreversibility of the unfolding transitions observed at the experimental conditions used, we report apparent T_m values (T_{mapp}).

Enzymatic hydrolysis assay

The enzymatic hydrolysis of cellulose was evaluated using 1.6% w/v carboxy-methyl cellulose (CMC), 0.4% w/v PASC and 3.8% w/v Avicel as substrate. The CenA^{CD}d concentrations used in these assays were 0.10 µM, 0.21 µM, and 1.75 µM for CMC, PASC, and Avicel hydrolysis, respectively, both for the complexed and non-complexed enzyme samples. The reactions were carried out in TBS-TC buffer at 40 °C under continuous stirring at 800 rpm on a Thermomixer (Dragon Lab, Beijing, China). Aliquots were extracted at different time intervals. The enzymatic reactions were stopped by cooling the samples on ice, centrifuged for 10 min at 5000 × g at 4 °C, and the reducing sugars in the supernatant were evaluated using the dinitrosalicylic acid (DNS) assay (Miller 1959; Breuil and Saddler 1985). For this, 150 µL of DNS were added to 100 µL of each sample and boiled for 10 min. The absorbance was then measured at 540 nm, and the reducing sugars were calculated using a calibration curve with glucose as standard.

Enzymatic stability assays

Thermostability assays of CenA^{CD}d isolated and coupled to cBLS were performed pre-incubating the samples at 40 °C in TBS-TC buffer for 48 h under continuous mixing at 800 rpm on a Thermomixer (Dragon Lab, Beijing, China). Aliquots were extracted at different time intervals, and the residual activity of CenA^{CD}d was evaluated by incubating the enzyme (0.10 µM) with 2% CMC in TBS-TC buffer for 10 min at 40 °C with continuous mixing at 800 rpm. The reducing sugars produced were then evaluated using the DNS assay, as described previously. The residual activity measured was expressed as percent of the original activity without treatment (time = 0 h).

Pull-down assays

Briefly, 0.35 µM of CenA^{CD}d free or complexed with cBLS (cBLS-CenA$^{CD}d_{(10)}$ complex) were incubated with 0.4% PASC or 1% Avicel in TBS-TC buffer under continuous mixing for 1 h at 4 °C. Samples were then centrifuged for 10 min at 12,000 × g. The supernatants containing unbound proteins were discarded, and the pellets were washed two times with TBS-TC buffer to remove the protein nonspecifically bound to cellulose. The pellets were resuspended in SDS-PAGE sample buffer, boiled for 5 min at 95 °C, centrifuged for 1 min at 12,000 × g, and analyzed by SDS-PAGE electrophoresis (Laemmli 1970) on a 12% T 3% C polyacrylamide gel. After staining, the intensities of the bands were analyzed with ImageJ software (Schneider et al. 2012). Control samples representing the total input of CenA^{CD}d and cBLS used in the binding assays were included as reference. In addition, a control sample of cBLS incubated with both cellulose substrates was also included to test the non-specific binding of the scaffold to cellulose.

Molecular modeling

The theoretical structures of CenA^{CD}d, cBLS, and the cBLS-CenA^{CD}d complex were modeled using Modeller version 9.25 (Sali and Blundell 1993) and Swiss-PdbViewer DeepView v4.1 (Guex and Peitsch 1997). c-BLS was modeled using the structures of *C. thermocellum* cohesin-2 from CipA (pdb code 2ccl chain A (Carvalho et al. 2007)) and *B.*

abortus lumazine synthase (pdb code 1XN1 (Klinke et al. 2005)) as templates. The theoretical structure of CenA^{CD}d was modeled using the structures of GH6 endoglucanase from *Mycobacterium tuberculosis* (pdb code 1uoz, chain A, 42% identity (Varrot et al. 2005)) and dockerin domain of Xyn10B from *C. thermocellum* (pdb code 2ccl, chain B, 97% identity (Carvalho et al. 2007)) as templates. In these models, the C-terminal ends of CenA and cohesin were joined to the N-terminal ends of dockerin and BLS, respectively, through a pentapeptide linker of sequence GSGSG. Finally, the CenA^{CD}d and cBLS interaction was modeled using the experimental structure of the dockerin-cohesin complex 2ccl as template to obtain the theoretical model of the cBLS-CenA^{CD}d complex.

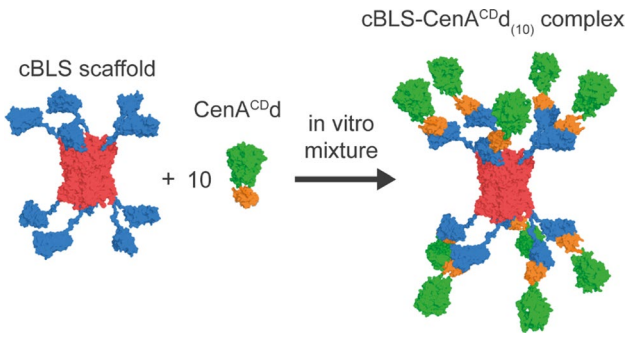

Fig. 1 Theoretical model of polymeric nanoparticles produced by the high affinity non-covalent interaction of heterodimeric cohesin (blue) and dockerin (orange) modules, complementary fused to the subunits of the decameric BLS scaffold (red) and endoglucanase CenA^{CD} (green), respectively. The theoretical structural models used in this figure were built as described in "Materials and methods" section

Results

Design of BLS multienzymatic complexes

The non-covalent coupling of proteins to oligomeric scaffolds is a convenient strategy for the production of multifunctional nanoparticles. This approach allows the independent folding of the scaffold and the target proteins. Coupling is achieved by mixing the complementary species after their independent expression and purification. Our group has previously developed strategies for the polymeric display of proteins on the structure of BLS through recombinant fusion or coiled coil interactions (Craig et al. 2005, 2012; Bellido et al. 2009; Mejias et al. 2013). Here we present a new method for the non-covalent coupling of proteins to BLS through high affinity heterodimeric cohesin and dockerin modules, and its use for the production of artificial cellulosomes (Fig. 1).

The coupling modules selected for our design were the cohesin domain 2 of CipA scaffolding protein and the dockerin domain of xylanase 10B, both from the cellulosome-producing bacteria *C. thermocellum.* This interaction pair has many features that make it convenient for engineering purposes. It has a high interaction strength ($K_a = 1.2 \times 10^{-8}$ M) (Carvalho et al. 2007), a high resolution crystallographic structure available of the complex (Carvalho et al. 2003, 2007), and belongs to a thermophilic microorganism.

In this work, we recombinantly fused cohesin to the N-terminal end of BLS (cBLS), and dockerin to a model enzyme. Due to the decameric nature of BLS, it would be expected that the cohesin domains fused to its structure would interact with up to 10 engineered enzymes fused to dockerin. Alternatively, wild type dockerin-bearing enzymes from *C. thermocellum* could be used without further engineering. The number of enzymes that could be coupled to the scaffold in the design roughly resembles the cellulosome architecture of *C. thermocellum*, in which 9 cohesin modules on the CipA scaffold interact with the dockerin domains of cellulolytic enzymes. We used *C. fimi* endoglucanase CenA as a model enzyme for the polymeric display on cBLS structure because it has been widely studied and has a good recombinant expression yield in bacteria (Raymond Wong et al. 1986; Gilkes et al. 1988, 1992). Wild type CenA is a monomeric non-cellulosomal endoglucanase (Shen et al. 1991) that contains a cellulose binding module (CBM) connected through a linker enriched in proline and threonine residues to a glycoside hydrolase family 6 catalytic domain. We recombinantly fused the selected dockerin domain of *C. thermocellum* to the C-terminus of the catalytic domain of CenA to produce the CenA^{CD}d fusion protein. The CBM module of the wild type enzyme was not included in the final construct. A flexible pentapeptide linker of sequence GSGSG was used to join the cohesin and BLS modules in cBLS, and CenA^{CD} and dockerin modules in CenA^{CD}d. This linker was used to give some separation between the fused modules and prevent their mutual interaction during folding, in a similar way as previously used in other BLS fusion proteins (Craig et al. 2012; Mejias et al. 2013). It would also provide some structural flexibility to the cBLS-CenA^{CD}d multienzymatic complex, which is an important feature that has been related to the ability of cellulosomes to adapt and degrade lignocellulosic substrates (Hammel et al. 2005).

Figure 1 shows a theoretical structural model of the complex between CenA^{CD}d and cBLS (cBLS-CenA^{CD}d complex). The model shows that there is enough space available in the cBLS scaffold to accommodate 10 CenA^{CD}d modules without any overlap or steric restriction. It is also important to note that the catalytic site of CenA^{CD}d and the dockerin domain fused to its structure are located on opposite sides of the enzyme, allowing its simultaneous interaction with the cBLS scaffold and the cellulose substrate.

Production and characterization of cBLS and CenA^{CD}d

The cBLS and CenA^{CD}d fusion proteins were cloned in a pET11a vector and expressed in *E. coli* BL21(DE3) at 30 °C and 20 °C, respectively. Significant amounts of both proteins were solubly expressed in the bacterial cytosol (Fig. 2a).

The purification of cBLS was carried out by a combination of anion exchange and size exclusion chromatography, whereas CenA^{CD}d was purified through Ni–NTA (nickel-nitrilotriacetic acid) affinity and size exclusion chromatography as described in the "Materials and methods" section. The yields of cBLS and CenA^{CD}d obtained at the end of the purification process were approximately 40 mg and 5 mg per liter of *E. coli* culture, respectively. The SDS-PAGE analysis of the purified proteins showed single bands with a mobility compatible with the theoretical Mr expected for the cBLS subunits (33.1 kDa) and CenA^{CD}d (39.7 kDa) in denaturing conditions (Fig. 2a).

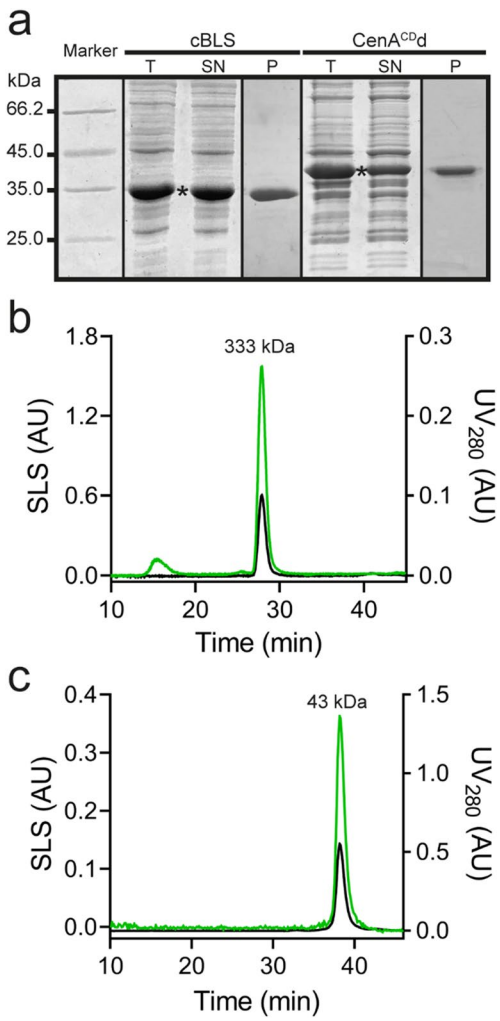

Fig. 2 Analysis of cBLS and CenA^{CD}d expressed in *E. coli*. Panel **a** SDS-PAGE analysis of the soluble (SN) and total (T) cellular fractions of the bacteria obtained after protein induction and cell lysis. The bands corresponding to each protein are labeled with a black asterisk. The analysis of the purified proteins (P) is also shown. The molecular mass marker is shown on the left side. Panel **b** and **c** correspond to the SEC-SLS analysis of purified cBLS and CenA^{CD}d, respectively. The proteins were loaded in a Superose 6 increase 10/300 GL column, and eluted with TBS-TC buffer at a flow rate of 0.5 mL/min. The elution was monitored by measuring the UV absorption at 280 nm (black line) and light scattering at 90° (green line) signals. The Mr calculated by SEC-SLS is indicated for each protein

In order to measure the Mr of these proteins in native conditions, and analyze their oligomeric state, we used the static light scattering coupled to size exclusion chromatography technique (SEC-SLS). In comparison with the Mr obtained through analysis of the retention time in SEC using calibration curves with Mr standards, the Mr calculated using SEC-SLS has no influence of the shape of the protein or its possible interaction with the column matrix. The SEC-SLS technique is a spectroscopic method that provides the absolute Mr of the protein species separated by SEC through the analysis of their SLS and UV signals. The SEC-SLS analysis of cBLS (Fig. 2b), showed a single homogenous peak of 333 ± 14 kDa (polydispersity index Mr/Mn~1.002), compatible with the theoretical Mr expected for the decameric BLS scaffold decorated with 10 cohesin modules (theoretical Mr of decameric cBLS: 331 kDa). This result suggests that the BLS modules are properly folded in the structure of cBLS. On the other hand, the SEC-SLS analysis of purified CenA^{CD}d (Fig. 2c) showed a single peak (polydispersity index Mr/Mn~1.004) with a Mr of 43 ± 1 kDa, compatible with the theoretical Mr of this protein in the monomeric state (39.7 kDa). No signs of aggregation were observed for cBLS and CenA^{CD}d in the SEC-SLS analysis of these proteins.

The cellulolytic activity of purified CenA^{CD}d, measured using CMC as substrate, was 408 mol of reducing sugars (as glucose) per mole of enzyme per min, similar to the activity reported in bibliography for the catalytic domain of CenA (280 mol of reducing sugars per mole of enzyme per min) (Meinke et al. 1993).

Overall, the results presented in this section, and the ability of CenA^{CD}d to interact with cBLS through their cohesin and dockerin modules, as will be shown in the following section, strongly support the structural and functional integrity of all the domains of both proteins.

Multienzymatic complex assembly and structural characterization

In order to test the non-covalent coupling of CenA^{CD}d to cBLS, we mixed both proteins in different molar ratios and analyzed the products obtained. The samples were incubated at 4 °C in TBS-TC buffer for 1 h to produce the coupling, although an incubation time of 10 min was generally enough to reach the binding equilibrium (data not shown). The SEC

analysis of the titration of cBLS with CenA^{CD}d (Fig. 3a) shows changes in the chromatographic profile of the scaffold that could be interpreted as a consequence of the incorporation of CenA^{CD}d to cBLS.

At increasing CenA^{CD}d concentration, an increase in the area and a decrease in the retention time of cBLS were observed as a consequence of CenA^{CD}d binding to the decameric scaffold (Fig. 3a). The coupling saturates at a molar ratio of approximately 1 CenA^{CD}d per cBLS subunit (Supplemental Fig. S1), which is compatible with the known 1:1 stoichiometric ratio of cohesin-dockerin complexes. After saturating all the cohesin sites of the scaffold (CenA^{CD}d/cBLS subunit molar ratios > 1), the retention time and the area of the peak corresponding to the multimeric complex remain constant, and an excess of free CenA^{CD}d starts to accumulate, as it is evident by the increase of the peak observed at a retention time of 38 min. No evidence of aggregation of the cBLS-CenA^{CD}d complex was observed, as there was no protein eluting at lower retention times or at the void volume of the column. The SEC-SLS analysis of the complex obtained in this saturating condition (Fig. 3b) showed a single homogeneous peak (polydispersity index Mr/Mn~1.003) of Mr 730 ± 1 kDa, compatible with the theoretical Mr of the cBLS-CenA^{CD}d$_{(10)}$ complex (728 kDa) produced by the binding of 10 CenA^{CD}d modules to the decameric structure of cBLS. The SDS-PAGE analysis of this peak confirmed the presence of equimolar amounts of two bands corresponding to cBLS and CenA^{CD}d subunits (inset Fig. 3b). These results demonstrate that all cohesin modules on the scaffold are functional, and that there is no significant steric hindrance for the colocalization of 10 CenA^{CD}d modules on the structure of the cBLS decameric scaffold.

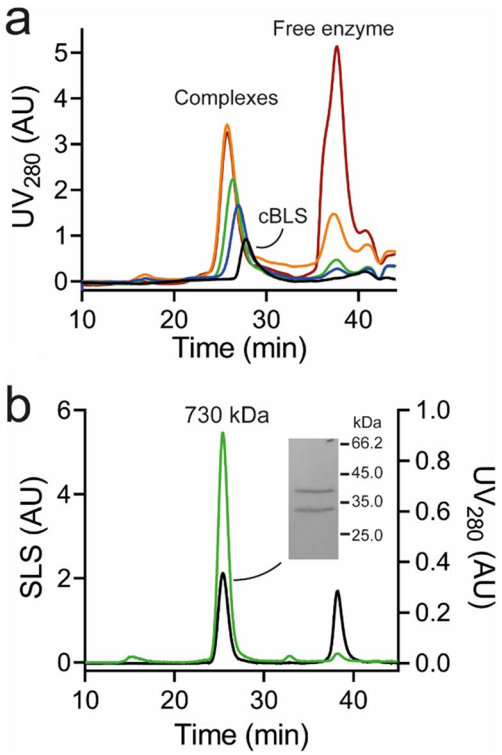

Fig. 3 Analysis of the binding titration of cBLS with CenA^{CD}d. Panel **a** shows the SEC analysis of 70 µg of cBLS incubated with increasing amounts of CenA^{CD}d at 0.3 (blue line), 0.6 (green line), 1.2 (orange line), and 2.4 (dark red line) CenA^{CD}d/cBLS molar ratios of protein subunits. The chromatographic profile of isolated cBLS is also shown as reference (black line). Panel **b** corresponds to the SEC-SLS analysis of the saturated cBLS-CenA^{CD}d complex prepared using a 2.0-fold molar excess of CenA^{CD}d over cBLS subunits. The samples were loaded in a Superose 6 increase 10/300 GL column, and eluted with TBS-TC buffer, at a flow rate of 0.5 mL/min. The elution was monitored by measuring the UV absorption at 280 nm (black line) and the light scattering at 90° (green line) signals. The inset in panel **b** shows the SDS-PAGE analysis of the elution peak corresponding to the saturated cBLS-CenA^{CD}d complex. The upper band corresponds to CenA^{CD}d and the lower one to cBLS

Conformational stability analysis

In order to evaluate the structural and conformational stability of the cBLS-CenA^{CD}d complex and its modules, we used circular dichroism (CD) spectroscopy.

The far UV-CD spectra of the isolated cBLS and CenA^{CD}d modules corresponded to those expected for properly folded proteins with alpha/beta structure (Fig. 4a). The spectrum of the cBLS-CenA^{CD}d$_{(10)}$ complex, prepared using equimolar amounts of CenA^{CD}d and cBLS subunits, was similar to the sum of the CD signals of the isolated modules. These results suggest that cBLS and CenA^{CD}d are properly folded in the structure of the complex, and that there is no significant change in the structure of the interacting modules upon binding.

The structural stability of cBLS-CenA^{CD}d$_{(10)}$, cBLS, and CenA^{CD}d was evaluated by measuring the heat induced denaturation curves of the complex and its modules through the analysis of the far UV-CD signal of each protein as a function of temperature (Fig. 4b and Supplemental Fig. S2). The results showed a high thermal stability for cBLS, which denatures in a single-step process with an apparent Tm of 85.5 °C, compatible with the thermal stability reported previously for decameric BLS (Tm ~ 88 °C (Zylberman et al. 2004)) and the cohesin module used in this construct (*C. thermocellum* cohesin-2 domain from CipA, Tm ~ 87 °C (Valbuena et al. 2009)). CenA^{CD}d showed lower stability. It cooperatively denatures in a single-step process with an apparent Tm of 54.0 °C, in agreement with the value reported for the catalytic module of CenA (Beadle et al. 1999). The absence of two transitions in the thermal unfolding curve of CenA^{CD}d suggests that the thermal stability of the dockerin domain of *C. thermocellum* Xyn10B used in this construct would be similar to that of the CenA catalytic

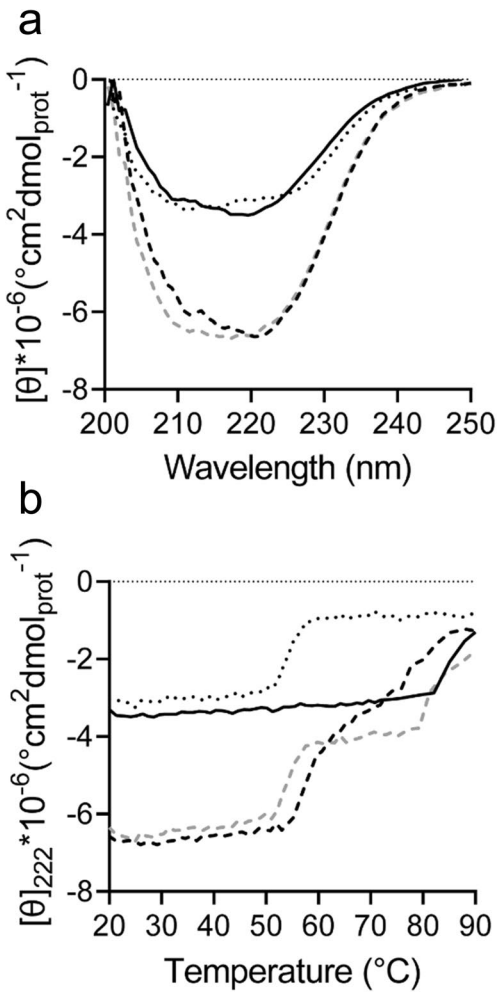

Fig. 4 CD spectroscopy analysis of cBLS-CenA^{CD}d complex and its isolated modules. Panel **a** shows the comparison of the far UV-CD spectra of CenA^{CD}d (black-dotted line), cBLS (black line), and the cBLS-CenA^{CD}d$_{(10)}$ complex (black-dashed line). The theoretical spectrum of cBLS-CenA^{CD}d$_{(10)}$ (gray dashed line), calculated from the sum of the CenA^{CD}d and cBLS spectra, is also shown for comparison. Panel **b** shows the thermal denaturation curves of CenA^{CD}d (black-dotted line), cBLS (black line), and the cBLS-CenA^{CD}d$_{(10)}$ complex (black-dashed line) evaluated by measuring the molar ellipticity at 222 nm of each protein sample as a function of temperature. The theoretical unfolding curve of the cBLS-CenA^{CD}d$_{(10)}$ complex, calculated from the sum of the CenA^{CD}d and cBLS curves, is also presented (gray dashed line). All measurements were done in TBS-TC buffer

module. Despite the lack of information about the structural stability of this dockerin domain, it is conceivable that it might be similar to that measured for the isolated dockerin module of the *C. thermocellum* Cel48S enzyme, which is stable at 55 °C in the presence of Ca^{+2} (Lytle et al. 2000). The heat-induced denaturation curve of cBLS-CenA^{CD}d$_{(10)}$ was more complex. Two major transitions were observed, compatible with the sequential thermal unfolding of the CenA^{CD}d and cBLS modules. The melting temperatures of these transitions were similar to those measured for the isolated proteins. However, some deviations from this trend were observed. Notably, the apparent Tm of CenA^{CD}d was increased from 54 to 58.3 °C upon binding to the complex. The cause of this increase is unknown, but it might be related to dockerin stabilization upon binding to the cohesin module of cBLS, or a stabilization of CenA^{CD}d produced by molecular crowding in the context of the polyvalent nanoparticle. By contrast, the apparent Tm of cBLS was decreased from 85.5 °C to approximately 77.6 °C probably due to a perturbation of its structure induced by denatured CenA^{CD}d. Overall, the results presented in this section indicate that the structure and stability of CenA^{CD}d were preserved in the structure of the complex.

Cellulose degradation activity of the polyvalent CenA^{CD}d complex is increased

To evaluate functional changes of CenA^{CD}d produced by its polyvalent display on the cBLS structure, we carried out a series of cellulose degradation reactions using exactly the same amount of CenA^{CD}d in the absence or presence of different amounts of cBLS. We used equimolar amounts of cBLS subunits and CenA^{CD}d for the production of complexes with 10 CenA^{CD}d enzymes per cBLS decamer (cBLS-CenA^{CD}d$_{(10)}$ complex), and a tenfold molar excess of cBLS subunits over CenA^{CD}d for the production of complexes with an average of 1 CenA^{CD}d per cBLS decamer (cBLS-CenA^{CD}d$_{(1)}$ complex). The activities of these complexes were compared to the activity of an equimolar amount of isolated CenA^{CD}d using CMC, PASC, and Avicel as model substrates for soluble, amorphous, and crystalline cellulose, respectively (Fig. 5).

The cellulose degradation of CenA^{CD}d was higher for CMC than for PASC, whereas the degradation of Avicel was significantly lower than the other substrates, in agreement with bibliographic data (Gilkes et al. 1988; Shen et al. 1991).

The cellulolytic activity of the monovalent complex cBLS-CenA^{CD}d$_{(1)}$ was not significantly different from that of free CenA^{CD}d for all substrates. Moreover, the decameric display of the enzyme produced no significant change in the degradation rate of CMC compared to equimolar amounts of the enzyme free in solution or in the monovalent complex. These results suggest no significant perturbation of the enzyme activity by steric factors that could arise as a consequence of its coupling to the scaffold. On the other hand, we observed a significant increase in the cellulose degradation activity of the decavalent complex cBLS-CenA^{CD}d$_{(10)}$ compared to the free enzyme and the monovalent complex, both for PASC and Avicel as substrates (Fig. 5). The increase in the amount of reducing sugars produced by the polyvalent complex compared to the free enzyme was ~ 70% for PASC, and ~ 40% for Avicel degradation. These results demonstrate

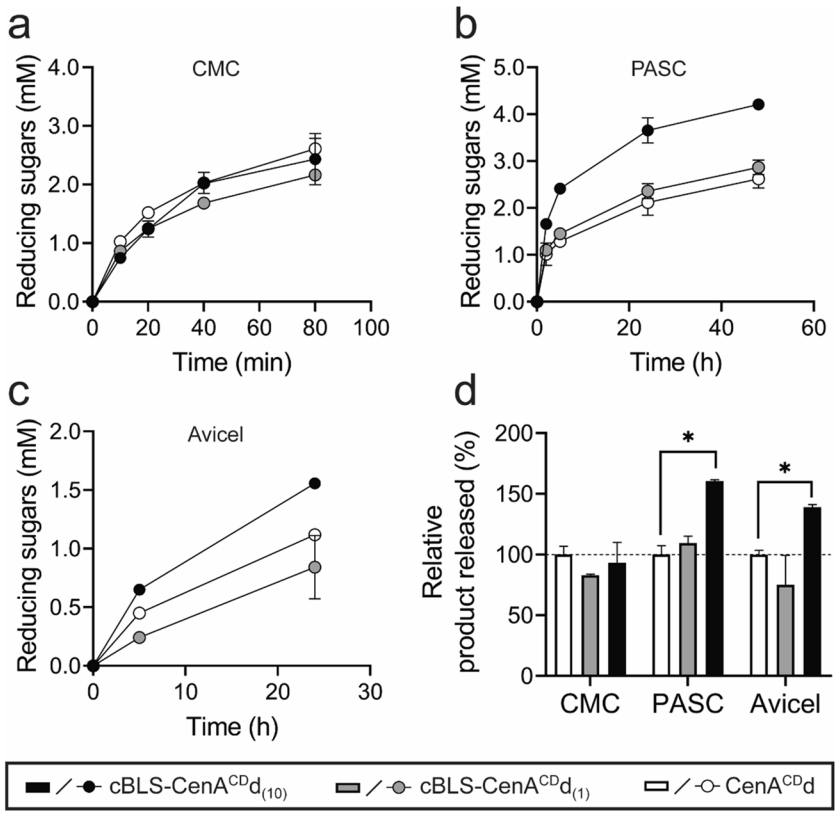

Fig. 5 Comparison of the amount of reducing sugars produced by complexed and non-complexed $CenA^{CD}d$. The product released by equimolar amounts of $CenA^{CD}d$ free in solution (white circles), in the monovalent complex cBLS-$CenA^{CD}d_{(1)}$ (gray circles), and in the polyvalent complex cBLS-$CenA^{CD}d_{(10)}$ (black circles), are shown. The reactions were carried out in TBS-TC buffer under continuous mixing at 40 °C. Panels **a**, **b**, and **c** show the degradation of 1.6% w/v CMC, 0.4% w/v PASC, and 3.8% w/v Avicel solutions, respectively. The reactions were evaluated by monitoring the release of reducing sugars equivalents (mM) over time, measured by the DNS method in the soluble fraction of the samples. The $CenA^{CD}d$ concentrations used for CMC, PASC, and Avicel hydrolysis were 0.10 μM, 0.21 μM, and 1.75 μM, respectively. The values reported represent the mean ± standard deviation of duplicate samples. Panel **d** compares the amount of product released at the last incubation time (80 min, 48 h, and 24 h for CMC, PASC, and Avicel, respectively) by free $CenA^{CD}d$ (white bars), cBLS-$CenA^{CD}d_{(1)}$ (gray bars), and cBLS-$CenA^{CD}d_{(10)}$ (black bars) for the different substrates used. The values are normalized using the product released by the free $CenA^{CD}d$ sample (2.6 mM, 2.6 mM, and 1.1 mM for CMC, PASC, and Avicel, respectively), used as 100% reference for each condition (marked with a dotted line). Asterisks denote statistically significant difference ($p < 0.05$) between cBLS-$CenA^{CD}d_{(10)}$ and $CenA^{CD}d$

that the polyvalent $CenA^{CD}d$ artificial cellulosome is superior for degrading cellulose insoluble substrates (PASC and Avicel) than the free enzyme, and that the functional gain observed is related to the multiplicity of enzymes coupled to the scaffold.

Residual activity of complexed and non-complexed $CenA^{CD}d$

In order to evaluate differences in the stability of complexed and non-complexed $CenA^{CD}d$ over time, we incubated $CenA^{CD}d$ and the cBLS-$CenA^{CD}d_{(10)}$ complex at 40 °C for 48 h, and measured the residual activity of aliquots extracted at different time intervals from each sample (Fig. 6).

We observed no difference in the residual activity of complexed and non-complexed $CenA^{CD}d$ in the time scale of the experiment. The residual activity after 48 h incubation at 40 °C was practically identical to the original one. These results suggest that the increment observed in the PASC and Avicel degradation activity of cBLS-$CenA^{CD}d_{(10)}$ compared to the free enzyme (Fig. 5) was not due to changes in the stability of the enzyme.

The polymeric display of $CenA^{CD}d$ increases the amount of enzyme associated to cellulose

Taking advantage of the insolubility of PASC and Avicel, we performed pull down assays to evaluate differences in the amount of enzyme associated to these substrates for the complexed and non-complexed forms of $CenA^{CD}d$. Samples with a constant amount of $CenA^{CD}d$ in the free state or complexed with cBLS (cBLS-$CenA^{CD}d_{(10)}$ complex) were incubated with

0.4% PASC or 1% Avicel in TBS-TC buffer under continuous mixing for 1 h at 4 °C. Under this condition, the degradation of the substrate is not significant. The fraction of protein associated to cellulose was separated by centrifugation, washed, redissolved in cracking buffer, and analyzed by SDS-PAGE (Fig. 7) as described in "Materials and methods" section. Control samples representing the total input of CenA^{CD}d and cBLS, and the non-specific binding of cBLS to cellulose were also included as reference in the assay.

The results observed for Avicel and PASC were similar. The analysis of the cBLS-CenA^{CD}d$_{(10)}$ sample showed two strong bands corresponding to CenA^{CD}d and cBLS (Fig. 7, lanes 1 and 4 for Avicel and PASC, respectively). The intensity of these bands was approximately 84% and 70% of the total load of these proteins in the assay for Avicel and PASC, respectively, suggesting an almost complete association of the cBLS-CenA^{CD}d$_{(10)}$ complex to both substrates. By contrast, a small amount of enzyme was observed in the pulldown of free CenA^{CD}d (Fig. 7, lanes 2 and 5 for Avicel and PASC, respectively), corresponding to a band intensity of ~ 16% compared to the total amount of CenA^{CD}d used in the assay (Fig. 7, lane 7). Finally, no binding of cBLS was observed (Fig. 7, lanes 3 and 6 for Avicel and PASC, respectively) indicating no interaction of the scaffold with the substrate.

In summary, the results presented in this section indicate that higher amounts of CenA^{CD}d are associated to cellulose when the enzyme is polyvalently displayed in the structure of the cBLS scaffold compared to an equimolar amount of the free enzyme. This increase may be attributed to an avidity effect produced as a consequence of the simultaneous interaction with cellulose of multiple CenA^{CD}d modules, producing a decrease in the apparent dissociation rate of the polyvalent complex from the substrate. Therefore, it is conceivable that the increased cellulose degradation activity of the polyvalent cBLS-CenA^{CD}d$_{(10)}$ complex formerly reported could be related to the increase observed in the amount of enzyme associated to the substrate.

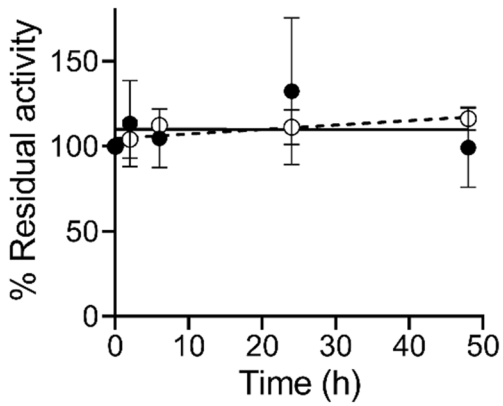

Fig. 6 Residual activity of complexed and non-complexed CenA^{CD}d. The figure shows the residual activity of CenA^{CD}d (empty circles) and cBLS-CenA^{CD}d$_{(10)}$ (black circles) over time at 40 °C. Enzyme samples were incubated in TBS-TC buffer under continuous agitation at 40 °C. The activity of aliquots of enzyme extracted at different time intervals was evaluated using 2% CMC as substrate and expressed as percentage of the initial incubation time. The values at each time point represent the mean ± standard deviation of duplicate samples. The linear regression of the residual activities of CenA^{CD}d and cBLS-CenA^{CD}d$_{(10)}$ over time is represented by a black-dashed line and a black line, respectively

Discussion

In this work, we introduced a new scaffold for the production of multifunctional particles based on the non-covalent coupling of target proteins to the structure of decameric BLS through the high affinity interaction of cohesin and dockerin modules recombinantly fused to BLS, and the target proteins, respectively. We illustrated the usefulness of this platform for the multivalent display of enzymes, using the catalytic domain of endoglucanase CenA from *C. fimi*, as a step forward to advance in the production of artificial cellulosomes.

The cBLS scaffold has many interesting properties for nanobiotechnological applications, namely its high recombinant expression yield in *E. coli*, multiplicity of coupling sites, and high thermal stability. These features open the possibility for the cost-effective production of this scaffold for multifunctional particle developments. The solubility and expression yield of cBLS could be attributed to the intrinsic properties of the cohesin and BLS modules used, and the self-assembly nature of the scaffold. These properties represent an advantage compared to the leu1-BLS scaffold previously developed in our group for the polymeric display of proteins, which is insolubly expressed as inclusion bodies in bacteria and needs a solubilization step in 8 M urea (Craig et al. 2012). It is also an advantage compared to natural cellulosome scaffolds, which are poorly expressed recombinantly in *E. coli* due to their repetitive nature and high molecular weight.

The decameric nature of cBLS allows the coupling of up to 10 dockerin bearing proteins to the cohesin modules of the scaffold. The results presented in this work show the successful production of multivalent cBLS-CenA^{CD}d complexes with different average compositions. The complete coupling of CenA^{CD}d to the 10 coupling sites of cBLS demonstrated the full functionality of the cohesin modules of the scaffold, and the lack of any significant steric hindrance for the polymeric display of enzymes of similar size.

In addition, we showed that cBLS is highly stable to thermal denaturation with an apparent Tm of 85 °C as measured by CD spectroscopy. This is an interesting

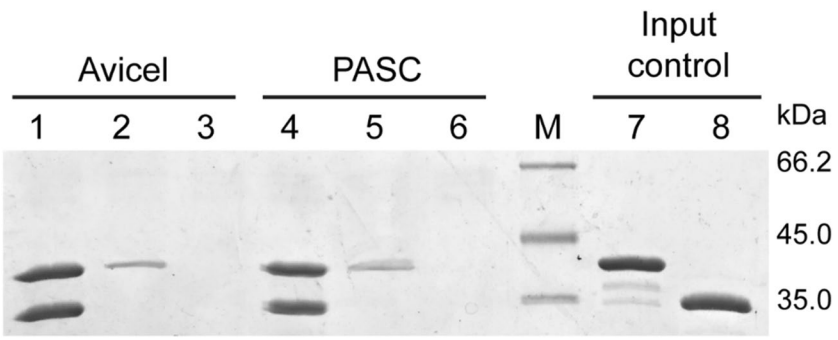

Fig. 7 SDS-PAGE analysis of pulldown assays with cellulose of complexed and non-complexed CenA^{CD}d. The figure shows the pulldown analysis of cBLS-CenA^{CD}d$_{(10)}$ and CenA^{CD}d for Avicel (lanes 1 and 2, respectively) and PASC (lanes 4 and 5, respectively). Samples with cBLS only were also included in the pulldown assay to test the non-specific binding of this protein to PASC (lane 3) and Avicel (lane 6). CenA^{CD}d and cBLS were also directly loaded in the gel without any further treatment (lanes 7 and 8, respectively), as a reference of the total amount of each protein used in the pulldown assays shown in lanes 1–6. The bands corresponding to CenA^{CD}d (39.7 kDa) and cBLS monomer (33.1 kDa) can be distinguished in the gel. Lane M corresponds to the molecular mass markers

feature that would allow the scaffolding of thermophilic enzymes for reactions at high temperature. The structural and functional stability of CenA^{CD}d was mostly preserved in the polyvalent cBLS-CenA^{CD}d$_{(10)}$ complex, and even a slight increase in apparent Tm of this module was observed.

Most importantly, the polymeric display of CenA^{CD}d using the cBLS scaffold produced a significant increase in the cellulose degradation activity of the cBLS-CenA^{CD}d$_{(10)}$ complex compared to the free enzyme (1.4- and 1.7-fold increase for the degradation of Avicel and PASC, respectively). By contrast, no increase in the degradation activity of the soluble CMC substrate was observed. The magnitude of the increase observed in the degradation of the crystalline (Avicel) and amorphous (PASC) insoluble substrates was similar to the one observed for other multienzymatic systems where single enzymes or restricted combinations of endoglucanases, exoglucanases, and cellulose binding domains were polyvalently displayed on structural scaffolds (Heyman et al. 2007; Mitsuzawa et al. 2009; Moraïs et al. 2010; Kim et al. 2012; Blanchette et al. 2012; Lu et al. 2019). However, higher functional improvements of approximately 4- to 12-fold have been observed for large artificial cellulosomes (Stern et al. 2016; Sun and Chen 2016; Chundawat et al. 2016) and full length cellulosomal scaffolds loaded with a high diversity of synergic enzymes (Krauss et al. 2012; Hirano et al. 2015, 2016; Leis et al. 2018). The functional enhancement of cellulolytic enzymes in natural and designed artificial cellulosomes is commonly attributed to enzyme targeting and proximity effects. Proximity effects are associated with the colocalization of enzymes in the same particle, whereas targeting effects are associated with the colocalization of cellulose binding modules with cellulolytic enzymes. Proximity of enzymes that catalyze sequential reactions could provide synergy through substrate channeling effects, increasing the local concentration of intermediate products and avoiding their diffusion to the bulk solvent (Zhang 2011; Moraïs et al. 2011). However, this is not the only molecular mechanism that could provide synergy through enzyme proximity. The increase in the degradation of the insoluble cellulosic substrates produced by the multivalent display of CenA^{CD}d using the cBLS scaffold could be attributed to an enzyme proximity effect. However, it is not related to a channeling effect because the system involves only a single type of enzyme. Our results suggest that the increase observed in the degradation rate of cellulose of the polyvalent enzyme compared to the monovalent one, is related to the increase produced in the amount of enzyme associated to the substrate. This phenomenon is most probably related to an avidity effect produced by the simultaneous binding of cellulose to multiple CenA^{CD}d modules on the same multienzymatic particle, increasing the enzyme concentration around the substrate. This retention phenomenon produced in the absence of any CBM intervention could be interpreted as a "targeting-like effect" or "pseudo targeting." The same type of phenomena was also described previously (Blanchette et al. 2012) for interpreting the increase observed in the cellulose degradation activity of a *Trichoderma viride* endoglucanase multivalently coupled to polystyrene particles.

The discrimination of this avidity phenomena produced by the colocalization of enzymes that degrade cellulose, from channeling and CBM mediated targeting effects, is important for the characterization of the molecular mechanisms of the cellulose degradation synergy observed in multienzymatic systems, and also for design purposes.

Whether the functional increase observed for the polyvalent CenA^{CD}d complex corresponds to a general

phenomenon and could occur with other endoglucanases merits further analysis. It is expected that this phenomenon would depend on the binding and catalytic properties, as well as the processive or non-processive nature of the enzymes coupled to the scaffold. The enzymatic processivity could be affected in multienzymatic complexes (Zajki-Zechmeister et al. 2021). However, diverse processive enzymes are commonly observed in natural cellulosomes (Leis et al. 2017). In this regard, it worth noting that endoglucanase CenA used in this work is a non-processive enzyme (Stålbrand et al. 1998; Uchiyama et al. 2020).

The strategy for the production of multienzymatic complexes using the cBLS scaffold presented in this paper could be adapted for the simultaneous colocalization of different cellulolytic enzymes, and cellulose binding domains, to advance the production of artificial cellulosomes. The colocalization of enzymes would be produced by mixing the different dockerin containing proteins with the cBLS scaffold. The stochastic assembly of enzymes with dockerin specificity matching the cohesin module of the scaffold would be conceptually similar to the assembly of natural cellulosomes, allowing flexibility in the ratio of enzymes assembled to the scaffold depending on the composition of the substrate to be degraded. It is expected that this technology would be valuable to improve lignocellulose degradation.

Supplementary Information The online version contains supplementary material available at https://doi.org/10.1007/s00253-023-12581-6.

Acknowledgements Thanks to Dr. Alejandro Nadra for providing the source material of the enzyme studied, Dr. Jimena Rinaldi for assistance in the SEC-SLS measurements, and Federico Vignale, Dr. Javier Santos, and Dr. Diana Wetzler for general assistance. Matias R. Iglesias Rando and Natalia Gorojovsky were supported by doctoral fellowships from CONICET.

Author contribution Author POC conceived and designed research. MRIR and NG conducted experiments. VZ and FAG contributed reagents and analytical tools. MRIR and POC analyzed data. MRIR and POC wrote the manuscript. All authors read and approved the final manuscript.

Funding This research was supported by grants to POC from UBACyT (2018: 20020170200244BA) and ANPCyT (PICT-2017–3925).

Data availability All data generated or analyzed during this study are included in this published article and its supplementary information files.

Declarations

Ethical approval This article does not contain any studies with human participants or animals performed by any of the authors.

Conflict of interest The authors declare no competing interests.

References

Agapakis CM, Boyle PM, Silver PA (2012) Natural strategies for the spatial optimization of metabolism in synthetic biology. Nat Chem Biol 8(6):527–535. https://doi.org/10.1038/nchembio.975

Alvarez P, Zylberman V, Ghersi G, Boado L, Palacios C, Goldbaum F, Mattion N (2013) Tandem repeats of the extracellular domain of Matrix 2 influenza protein exposed in *Brucella* lumazine synthase decameric carrier molecule induce protection in mice. Vaccine 31(5):806–812. https://doi.org/10.1016/j.vaccine.2012.11.072

Arfi Y, Shamshoum M, Rogachev I, Peleg Y, Bayer EA (2014) Integration of bacterial lytic polysaccharide monooxygenases into designer cellulosomes promotes enhanced cellulose degradation. Proc Natl Acad Sci 111(25):9109–9114. https://doi.org/10.1073/pnas.1404148111

Artzi L, Bayer EA, Moraïs S (2017) Cellulosomes: bacterial nanomachines for dismantling plant polysaccharides. Nat Rev Microbiol 15(2):83–95. https://doi.org/10.1038/nrmicro.2016.164

Banerjee D, Liu AP, Voss N, Schmid SL, Finn MG (2010) Multivalent display and receptor-mediated endocytosis of transferrin on virus-like particles. Chembiochem Eur J Chem Biol 11(9):1273–1279. https://doi.org/10.1002/cbic.201000125

Bayer EA (2017) Cellulosomes and designer cellulosomes: why toy with Nature? Environ Microbiol Rep 9(1):14–15. https://doi.org/10.1111/1758-2229.12489

Bayer EA, Kenig R, Lamed R (1983) Adherence of *Clostridium thermocellum* to cellulose. J Bacteriol 156(2):818–827

Beadle BM, Baase WA, Wilson DB, Gilkes NR, Shoichet BK (1999) Comparing the thermodynamic stabilities of a related thermophilic and mesophilic enzyme. Biochemistry 38(8):2570–2576. https://doi.org/10.1021/bi9824902

Bellido D, Craig PO, Mozgovoj MV, Gonzalez DD, Wigdorovitz A, Goldbaum FA, Dus Santos MJ (2009) *Brucella* spp. lumazine synthase as a bovine rotavirus antigen delivery system. Vaccine 27(1):136–145. https://doi.org/10.1016/j.vaccine.2008.10.018

Berguer PM, Blaustein M, Bredeston LM, Craig PO, D'Alessio C, Elias F, Farré PC, Fernández NB, Gentili HG, Gándola YB, Gasulla J, Gudesblat GE, Herrera MG, Ibañez LI, Idrovo-Hidalgo T, Nadra AD, Noseda DG, Paván CH, Pavan MF, Pignataro MF, Roman EA, Ruberto LAM, Rubinstein N, Sanchez MV, Santos J, Wetzler DE, Zelada AM, Argentinian AntiCovid Consortium (2022) Covalent coupling of Spike's receptor binding domain to a multimeric carrier produces a high immune response against SARS-CoV-2. Sci Rep 12(1):692. https://doi.org/10.1038/s41598-021-03675-0

Blanchette C, Lacayo CI, Fischer NO, Hwang M, Thelen MP (2012) Enhanced cellulose degradation using cellulase-nanosphere complexes. PLOS ONE 7(8):e42116. https://doi.org/10.1371/journal.pone.0042116

Bonomi HR, Marchesini MI, Klinke S, Ugalde JE, Zylberman V, Ugalde RA, Comerci DJ, Goldbaum FA (2010) An atypical riboflavin pathway is essential for *Brucella abortus* virulence. PLOS ONE 5(2):e9435. https://doi.org/10.1371/journal.pone.0009435

Breuil C, Saddler JN (1985) Comparison of the 3,5-dinitrosalicylic acid and Nelson-Somogyi methods of assaying for reducing sugars and determining cellulase activity. Enzyme Microb Technol 7(7):327–332. https://doi.org/10.1016/0141-0229(85)90111-5

Carvalho AL, Dias FMV, Prates JAM, Nagy T, Gilbert HJ, Davies GJ, Ferreira LMA, Romão MJ, Fontes CMGA (2003) Cellulosome assembly revealed by the crystal structure of the cohesin–dockerin complex. Proc Natl Acad Sci 100(24):13809–13814. https://doi.org/10.1073/pnas.1936124100

Carvalho AL, Dias FMV, Nagy T, Prates JAM, Proctor MR, Smith N, Bayer EA, Davies GJ, Ferreira LMA, Romão MJ, Fontes

CMGA, Gilbert HJ (2007) Evidence for a dual binding mode of dockerin modules to cohesins. Proc Natl Acad Sci 104(9):3089–3094. https://doi.org/10.1073/pnas.0611173104

Chundawat SPS, Paavola CD, Raman B, Nouailler M, Chan SL, Mielenz JR, Receveur-Brechot V, Trent JD, Dale BE (2016) Saccharification of thermochemically pretreated cellulosic biomass using native and engineered cellulosomal enzyme systems. React Chem Eng 1(6):616–628. https://doi.org/10.1039/C6RE00172F

Craig PO, Berguer PM, Ainciart N, Zylberman V, Thomas MG, Tosar LJM, Bulloj A, Boccaccio GL, Goldbaum FA (2005) Multiple display of a protein domain on a bacterial polymeric scaffold. Proteins Struct Funct Bioinforma 61(4):1089–1100. https://doi.org/10.1002/prot.20635

Craig PO, Alzogaray V, Goldbaum FA (2012) Polymeric display of proteins through high affinity leucine zipper peptide adaptors. Biomacromol 13(4):1112–1121. https://doi.org/10.1021/bm201875p

Davidi L, Moraïs S, Artzi L, Knop D, Hadar Y, Arfi Y, Bayer EA (2016) Toward combined delignification and saccharification of wheat straw by a laccase-containing designer cellulosome. Proc Natl Acad Sci 113(39):10854–10859. https://doi.org/10.1073/pnas.1608012113

Dueber JE, Wu GC, Malmirchegini GR, Moon TS, Petzold CJ, Ullal AV, Prather KLJ, Keasling JD (2009) Synthetic protein scaffolds provide modular control over metabolic flux. Nat Biotechnol 27(8):753–759. https://doi.org/10.1038/nbt.1557

Garbett D, Bretscher A (2014) The surprising dynamics of scaffolding proteins. Mol Biol Cell 25(16):2315–2319. https://doi.org/10.1091/mbc.e14-04-0878

Gestwicki JE, Cairo CW, Strong LE, Oetjen KA, Kiessling LL (2002) Influencing receptor−ligand binding mechanisms with multivalent ligand architecture. J Am Chem Soc 124(50):14922–14933. https://doi.org/10.1021/ja027184x

Gilkes NR, Warren RA, Miller RC, Kilburn DG (1988) Precise excision of the cellulose binding domains from two *Cellulomonas fimi* cellulases by a homologous protease and the effect on catalysis. J Biol Chem 263(21):10401–10407

Gilkes NR, Jervis E, Henrissat B, Tekant B, Miller RC, Warren RA, Kilburn DG (1992) The adsorption of a bacterial cellulase and its two isolated domains to crystalline cellulose. J Biol Chem 267(10):6743–6749

Guex N, Peitsch MC (1997) SWISS-MODEL and the Swiss-PdbViewer: an environment for comparative protein modeling. Electrophoresis 18(15):2714–2723. https://doi.org/10.1002/elps.1150181505

Gunnoo M, Cazade P-A, Galera-Prat A, Nash MA, Czjzek M, Cieplak M, Alvarez B, Aguilar M, Karpol A, Gaub H, Carrión-Vázquez M, Bayer EA, Thompson D (2016) Nanoscale engineering of designer cellulosomes. Adv Mater 28(27):5619–5647. https://doi.org/10.1002/adma.201503948

Hammel M, Fierobe H-P, Czjzek M, Kurkal V, Smith JC, Bayer EA, Finet S, Receveur-Bréchot V (2005) Structural basis of cellulosome efficiency explored by small angle X-ray scattering. J Biol Chem 280(46):38562–38568. https://doi.org/10.1074/jbc.M503168200

Heyman A, Barak Y, Caspi J, Wilson DB, Altman A, Bayer EA, Shoseyov O (2007) Multiple display of catalytic modules on a protein scaffold: nano-fabrication of enzyme particles. J Biotechnol 131(4):433–439. https://doi.org/10.1016/j.jbiotec.2007.07.940

Himmel ME, Ding S-Y, Johnson DK, Adney WS, Nimlos MR, Brady JW, Foust TD (2007) Biomass recalcitrance: engineering plants and enzymes for biofuels production. Science 315(5813):804–807. https://doi.org/10.1126/science.1137016

Hirano K, Nihei S, Hasegawa H, Haruki M, Hirano N (2015) Stoichiometric assembly of the cellulosome generates maximum synergy for the degradation of crystalline cellulose, as revealed by in vitro reconstitution of the *Clostridium thermocellum* cellulosome. Appl Environ Microbiol 81(14):4756–4766. https://doi.org/10.1128/AEM.00772-15

Hirano K, Kurosaki M, Nihei S, Hasegawa H, Shinoda S, Haruki M, Hirano N (2016) Enzymatic diversity of the *Clostridium thermocellum* cellulosome is crucial for the degradation of crystalline cellulose and plant biomass. Sci Rep 6(1):35709. https://doi.org/10.1038/srep35709

Hiriart Y, Rossi AH, Biedma ME, Errea AJ, Moreno G, Cayet D, Rinaldi J, Blancá B, Sirard JC, Goldbaum F, Berguer P, Rumbo M (2017) Characterization of structural and immunological properties of a fusion protein between flagellin from *Salmonella* and lumazine synthase from *Brucella*. Protein Sci 26(5):1049–1059. https://doi.org/10.1002/pro.3151

Jennings GT, Bachmann MF (2008) The coming of age of virus-like particle vaccines. Biol Chem 389(5):521–536. https://doi.org/10.1515/BC.2008.064

Jørgensen K, Rasmussen AV, Morant M, Nielsen AH, Bjarnholt N, Zagrobelny M, Bak S, Møller BL (2005) Metabolon formation and metabolic channeling in the biosynthesis of plant natural products. Curr Opin Plant Biol 8(3):280–291. https://doi.org/10.1016/j.pbi.2005.03.014

Kim D-M, Nakazawa H, Umetsu M, Matsuyama T, Ishida N, Ikeuchi A, Takahashi H, Asano R, Kumagai I (2012) A nanocluster design for the construction of artificial cellulosomes. Catal Sci Technol 2(3):499–503. https://doi.org/10.1039/C2CY00371F

Klinke S, Zylberman V, Vega DR, Guimarães BG, Braden BC, Goldbaum FA (2005) Crystallographic studies on decameric *Brucella spp.* lumazine synthase: a novel quaternary arrangement evolved for a new function? J Mol Biol 353(1):124–137. https://doi.org/10.1016/j.jmb.2005.08.017

Klinke S, Zylberman V, Bonomi HR, Haase I, Guimarães BG, Braden BC, Bacher A, Fischer M, Goldbaum FA (2007) Structural and kinetic properties of lumazine synthase isoenzymes in the order Rhizobiales. J Mol Biol 373(3):664–680. https://doi.org/10.1016/j.jmb.2007.08.021

Krauss J, Zverlov VV, Schwarz WH (2012) In vitro reconstitution of the complete *Clostridium thermocellum* cellulosome and synergistic activity on crystalline cellulose. Appl Environ Microbiol 78(12):4301–4307. https://doi.org/10.1128/AEM.07959-11

Laemmli UK (1970) Cleavage of structural proteins during the assembly of the head of bacteriophage T4. Nature 227(5259):680–685. https://doi.org/10.1038/227680a0

Laplagne DA, Zylberman V, Ainciart N, Steward MW, Sciutto E, Fossati CA, Goldbaum FA (2004) Engineering of a polymeric bacterial protein as a scaffold for the multiple display of peptides. Proteins Struct Funct Bioinforma 57(4):820–828. https://doi.org/10.1002/prot.20248

Leis B, Held C, Bergkemper F, Dennemarck K, Steinbauer R, Reiter A, Mechelke M, Moerch M, Graubner S, Liebl W, Schwarz WH, Zverlov VV (2017) Comparative characterization of all cellulosomal cellulases from *Clostridium thermocellum* reveals high diversity in endoglucanase product formation essential for complex activity. Biotechnol Biofuels 10:240. https://doi.org/10.1186/s13068-017-0928-4

Leis B, Held C, Andreeßen B, Liebl W, Graubner S, Schulte L-P, Schwarz WH, Zverlov VV (2018) Optimizing the composition of a synthetic cellulosome complex for the hydrolysis of softwood pulp: identification of the enzymatic core functions and biochemical complex characterization. Biotechnol Biofuels 11(1):220. https://doi.org/10.1186/s13068-018-1220-y

Lu L, Zhang L, Yuan L, Zhu T, Chen W, Wang G, Wang Q (2019) Artificial cellulosome complex from the self-assembly of Ni-NTA-functionalized polymeric micelles and cellulases. ChemBioChem 20(11):1394–1399. https://doi.org/10.1002/cbic.201900061

Ludwig C, Wagner R (2007) Virus-like particles—universal molecular toolboxes. Curr Opin Biotechnol 18(6):537–545. https://doi.org/10.1016/j.copbio.2007.10.013

Lytle BL, Volkman BF, Westler WM, Wu JH (2000) Secondary structure and calcium-induced folding of the *Clostridium thermocellum* dockerin domain determined by NMR spectroscopy. Arch Biochem Biophys 379(2):237–244. https://doi.org/10.1006/abbi.2000.1882

Meinke A, Gilkes NR, Kilburn DG, Miller RC, Warren RA (1993) Cellulose-binding polypeptides from *Cellulomonas fimi*: endoglucanase D (CenD), a family A beta-1,4-glucanase. J Bacteriol 175(7):1910–1918. https://doi.org/10.1128/jb.175.7.1910-1918.1993

Mejía-Méndez JL, Vazquez-Duhalt R, Hernández LR, Sánchez-Arreola E, Bach H (2022) Virus-like particles: fundamentals and biomedical applications. Int J Mol Sci 23(15):8579. https://doi.org/10.3390/ijms23158579

Mejias MP, Ghersi G, Craig PO, Panek CA, Bentancor LV, Baschkier A, Goldbaum FA, Zylberman V, Palermo MS (2013) Immunization with a chimera consisting of the B subunit of shiga toxin type 2 and *Brucella* lumazine synthase confers total protection against Shiga toxins in mice. J Immunol 191(5):2403–2411. https://doi.org/10.4049/jimmunol.1300999

Miller GL (1959) Use of dinitrosalicylic acid reagent for determination of reducing sugar. Anal Chem 31(3):426–428. https://doi.org/10.1021/ac60147a030

Mingardon F, Chanal A, López-Contreras AM, Dray C, Bayer EA, Fierobe H-P (2007) Incorporation of fungal cellulases in bacterial minicellulosomes yields viable, synergistically acting cellulolytic complexes. Appl Environ Microbiol 73(12):3822–3832. https://doi.org/10.1128/AEM.00398-07

Mingardon F, Chanal A, Tardif C, Bayer EA, Fierobe H-P (2007) Exploration of new geometries in cellulosome-like chimeras. Appl Environ Microbiol 73(22):7138–7149. https://doi.org/10.1128/AEM.01306-07

Mitsuzawa S, Kagawa H, Li Y, Chan SL, Paavola CD, Trent JD (2009) The rosettazyme: a synthetic cellulosome. J Biotechnol 143(2):139–144. https://doi.org/10.1016/j.jbiotec.2009.06.019

Moraïs S, Heyman A, Barak Y, Caspi J, Wilson DB, Lamed R, Shoseyov O, Bayer EA (2010) Enhanced cellulose degradation by nano-complexed enzymes: synergism between a scaffold-linked exoglucanase and a free endoglucanase. J Biotechnol 147(3–4):205–211. https://doi.org/10.1016/j.jbiotec.2010.04.012

Moraïs S, Barak Y, Hadar Y, Wilson DB, Shoham Y, Lamed R, Bayer EA (2011) Assembly of xylanases into designer cellulosomes promotes efficient hydrolysis of the xylan component of a natural recalcitrant cellulosic substrate. mBio 2(6):e00233-11. https://doi.org/10.1128/mBio.00233-11

Moraïs S, Morag E, Barak Y, Goldman D, Hadar Y, Lamed R, Shoham Y, Wilson DB, Bayer EA (2012) Deconstruction of lignocellulose into soluble sugars by native and designer cellulosomes. mBio 3(6):e00508-12. https://doi.org/10.1128/mBio.00508-12

Plückthun A, Pack P (1997) New protein engineering approaches to multivalent and bispecific antibody fragments. Immunotechnology 3(2):83–105. https://doi.org/10.1016/S1380-2933(97)00067-5

Raymond Wong WK, Gerhard B, Guo ZM, Kilburn DG, Anthony R, Warren J, Miller RC (1986) Characterization and structure of an endoglucanase gene cenA of *Cellulomonas fimi*. Gene 44(2):315–324. https://doi.org/10.1016/0378-1119(86)90196-4

Rossi AH, Farias A, Fernández JE, Bonomi HR, Goldbaum FA, Berguer PM (2015) *Brucella spp.* lumazine synthase induces a TLR4-mediated protective response against B16 melanoma in mice. PLOS ONE 10(5):e0126827. https://doi.org/10.1371/journal.pone.0126827

Sali A, Blundell TL (1993) Comparative protein modelling by satisfaction of spatial restraints. J Mol Biol 234(3):779–815. https://doi.org/10.1006/jmbi.1993.1626

Schneider CA, Rasband WS, Eliceiri KW (2012) NIH Image to ImageJ: 25 years of image analysis. Nat Methods 9(7):671–675. https://doi.org/10.1038/nmeth.2089

Shen H, Schmuck M, Pilz I, Gilkes NR, Kilburn DG, Miller RC, Warren RA (1991) Deletion of the linker connecting the catalytic and cellulose-binding domains of endoglucanase A (CenA) of *Cellulomonas fimi* alters its conformation and catalytic activity. J Biol Chem 266(17):11335–11340

Shoham Y, Lamed R, Bayer EA (1999) The cellulosome concept as an efficient microbial strategy for the degradation of insoluble polysaccharides. Trends Microbiol 7(7):275–281. https://doi.org/10.1016/S0966-842X(99)01533-4

Stålbrand H, Mansfield SD, Saddler JN, Kilburn DG, Warren RA, Gilkes NR (1998) Analysis of molecular size distributions of cellulose molecules during hydrolysis of cellulose by recombinant *Cellulomonas fimi* beta-1,4-glucanases. Appl Environ Microbiol 64:2374–2379. https://doi.org/10.1128/AEM.64.7.2374-2379.1998

Stern J, Moraïs S, Lamed R, Bayer EA (2016) Adaptor scaffoldins: an original strategy for extended designer cellulosomes, inspired from nature. mBio 7(2):e00083-16. https://doi.org/10.1128/mBio.00083-16

Sun Q, Chen W (2016) HaloTag mediated artificial cellulosome assembly on a rolling circle amplification DNA template for efficient cellulose hydrolysis. Chem Commun Camb Engl 52(40):6701–6704. https://doi.org/10.1039/c6cc02035f

Sun Q, Madan B, Tsai S-L, DeLisa MP, Chen W (2014) Creation of artificial cellulosomes on DNA scaffolds by zinc finger protein-guided assembly for efficient cellulose hydrolysis. Chem Commun Camb Engl 50(12):1423–1425. https://doi.org/10.1039/c3cc47215a

Uchiyama T, Uchihashi T, Nakamura A, Watanabe H, Kaneko S, Samejima M, Igarashi K (2020) Convergent evolution of processivity in bacterial and fungal cellulases. Proc Natl Acad Sci U S A 117:19896–19903. https://doi.org/10.1073/pnas.2011366117

Valbuena A, Oroz J, Hervás R, Vera AM, Rodríguez D, Menéndez M, Sulkowska JI, Cieplak M, Carrión-Vázquez M (2009) On the remarkable mechanostability of scaffoldins and the mechanical clamp motif. Proc Natl Acad Sci U S A 106(33):13791–13796. https://doi.org/10.1073/pnas.0813093106

Varrot A, Leydier S, Pell G, Macdonald JM, Stick RV, Henrissat B, Gilbert HJ, Davies GJ (2005) *Mycobacterium tuberculosis* strains possess functional cellulases. J Biol Chem 280(21):20181–20184. https://doi.org/10.1074/jbc.C500142200

Wilson DB (2009) Cellulases and biofuels. Curr Opin Biotechnol 20(3):295–299. https://doi.org/10.1016/j.copbio.2009.05.007

You C, Zhang Y-HP (2014) Annexation of a high-activity enzyme in a synthetic three-enzyme complex greatly decreases the degree of substrate channeling. ACS Synth Biol 3(6):380–386. https://doi.org/10.1021/sb4000993

Zajki-Zechmeister K, Kaira GS, Eibinger M, Seelich K, Nidetzky B (2021) Processive enzymes kept on a leash: how cellulase activity in multienzyme complexes directs nanoscale deconstruction of cellulose. ACS Catal 11:13530–13542. https://doi.org/10.1021/acscatal.1c03465

Zhang Y-HP (2011) Substrate channeling and enzyme complexes for biotechnological applications. Biotechnol Adv 29(6):715–725. https://doi.org/10.1016/j.biotechadv.2011.05.020

Zhang J, Tanha J, Hirama T, Khieu NH, To R, Tong-Sevinc H, Stone E, Brisson J-R, Roger MacKenzie C (2004) Pentamerization of single-domain antibodies from phage libraries: a novel strategy for the rapid generation of high-avidity antibody reagents. J Mol Biol 335(1):49–56. https://doi.org/10.1016/j.jmb.2003.09.034

Zylberman V, Craig PO, Klinke S, Braden BC, Cauerhff A, Goldbaum FA (2004) High order quaternary arrangement confers increased structural stability to *Brucella* sp. lumazine synthase. J Biol Chem 279(9):8093–8101. https://doi.org/10.1074/jbc.M312035200